JOURNAL OF PROPULSION AND POWER
Vol. 20, No. 5, September–October 2004

Analysis of the Magnetohydrodynamic Energy Bypass Engine for High-Speed Airbreathing Propulsion

David W. Riggins*
University of Missouri–Rolla, Rolla, Missouri 65409

The performance of the magnetohydrodynamic (MHD) energy bypass airbreathing engine for high-speed propulsion is analyzed. The general relationship between performance and overall total pressure ratio through an engine is described. Engines with large total pressure decreases, regardless of cause, have exponentially decreasing performance. The ideal inverse engine is demonstrated to have a significant total pressure decrease which is cycle-driven, degrades with energy bypassed, and is independent of any irreversibility. The ideal MHD engine (inverse engine with no irreversibility except in MHD work interactions) is next examined and has an additional large total pressure decrease. Fundamental characteristics of MHD engine flows from the standpoint of irreversibility are examined. Severe constraints exist on allowable deceleration Mach numbers and required component volume due to both losses and flow choking. Last, thermally balanced engine simulations utilizing inlet shock systems, chemistry, wall cooling, fuel injection and mixing, friction, etc., are summarized for both the MHD engine and the conventional scramjet. The MHD bypass engine has significantly lower performance across the Mach number range (8–12.2) due to 1) additional irreversibility and cooling requirements associated with the MHD components and 2) total pressure decrease associated with the inverse cycle itself.

Nomenclature

A	=	cross-sectional area, m^2
a	=	speed of sound, m/s
B	=	magnetic field strength, Wb/m^2
C_f	=	skin-friction coefficient (based on local dynamic pressure)
C_P	=	specific heat—constant pressure, J/kg · K
E_y	=	electrical field strength, N/C
F	=	engine thrust, N
f	=	fuel–air mass flow rate ratio
g_0	=	gravitational acceleration at sea level, m/s^2
h	=	lower heating value of fuel, J/kg (fuel); enthalpy, J/kg
I_{sp}	=	engine specific impulse
M	=	flow Mach number
mw	=	molecular weight
P	=	pressure, N/m^2
Q	=	heat added per mass of air, J/kg
R	=	gas constant, J/kg · K
S, s	=	entropy per mass, J/kg · K
T	=	temperature, K
u	=	fluid velocity, m/s
V	=	component volume, m^3
W	=	magnitude of component work interaction per mass of air, J/kg
x	=	exponential factor in magnetohydrodynamics work interaction
α_l	=	species l mass fraction
β	=	energy bypass ratio, $W(\text{extract})/C_P T_{ti}$
γ	=	ratio of specific heata
η	=	second-law effectiveness (also known as load factor), uB/E_Y
ρ	=	fluid density, kg/m^3
σ_0	=	electrical conductivity, mho/m

Subscripts

e	=	engine exit
eff	=	flow based
i	=	engine entrance
irr	=	irreversibility
surr	=	surroundings based
t	=	total
0	=	freestream

Introduction

FROM the standpoint of engine performance, the successful design of high-speed airbreathing engines is largely driven by adequately balancing the negative impact of irreversibility occurring in the flowpath (inevitably very large at high flight Mach numbers) with the positive impact of combustion-generated heat release (along with any fuel injection stream thrust).[1,2] There are a number of related design issues that affect design and performance as well. These include cycle effects on thermal efficiency, overall heat load and fuel capacity, local heat loads, the degree of disassociation occurring in the engine, flowpath configuration parameters, that is, area ratios, etc. This investigation focuses on analyzing and clarifying these and other design and performance issues for the specific case of the magnetohydrodynamics (MHD) energy bypass engine concept. In addition, the performance of the MHD bypass engine is contrasted with the conventional scramjet engine concept across a range of Mach numbers.

The aerospace Brayton cycle can be used to describe a wide range of engine flowfields, including turbojets, ramjets, and scramjets. For a more detailed and fundamental description of the thermodynamic performance-based continuum of single-stream airbreathing engines, see Riggins.[3] The turbojet cycle is based on work addition (mechanical compression) upstream of the burner along with (equal) downstream work extraction via mechanical turbines. The turbojet represents the basic (conventional) aerospace Brayton cycle. It is easily shown that, in the absence of all other issues, maximum overall engine efficiency mandates the maximum possible upstream work addition, that is, compression, at any flight condition. Related directly to this statement is that the total pressure ratio across the turbojet flowfield (exit to inlet) is greater than 1.0 and increases with increasing upstream work interaction. However, material thermal limits at combustor exit and chemical (disassociation) effects limit the actual compression allowable in a turbojet engine.

Received 4 September 2003; revision received 9 December 2003; accepted for publication 13 December 2003.

*Professor, Department of Mechanical and Aerospace Engineering. Senior Member AIAA.

In addition, as flight Mach number is increased and the total pressures and temperatures at the end of the inlet diffusion increase (due to increasing freestream kinetic energy), the amount of allowable upstream work addition decreases due to these same thermal and chemical limits, that is, the net total temperature rise associated with both compressor and burner is limited by the combustor exit temperature limit. The use of mechanical compressors and turbines also becomes increasingly problematic at high speeds. Eventually, at high supersonic flight Mach number, the ramjet, which has no work interaction devices, is preferred.

As flight Mach number increases further, the achievement of subsonic combustion in a ramjet becomes increasingly difficult. This is due to thermal and chemical limits and the inlet diffusion required for obtaining subsonic flow in the burner. The scramjet concept (supersonic combustion ramjet) reduces both inlet diffusion required as well as static temperatures in the engine core by achieving combustion at supersonic flowpath velocities. However, even for the scramjet, the core enthalpies experienced at high flight Mach number are very large, and hence, the scramjet requires the use of fuel as a thermal heat sink for surface cooling. This leads to injected fuel equivalence ratios larger than one. Irreversibility associated with supersonic mixing and combustion enhancement techniques also is significant. In addition, for any engine concept, as flight Mach number is increased, the ratio of energy per mass of air released by chemical combustion to the total enthalpy per mass of air entering the engine becomes very small, which results in rapidly decreasing thrust–drag margins for the vehicle.

Because of the high total enthalpy and the large core flow losses in the scramjet engine, the so-called inverse cycle jet engine has been proposed for high-speed airbreathing flight.[4–6] The inverse cycle can be viewed as a type (or variant) of the Brayton cycle. In this investigation, the inverse cycle concept is specialized to the case in which energy is extracted from the flowfield upstream of the burner and is then returned downstream of the burner. Depending on the amount of bypassed energy, the core of the engine (the combustor) may operate at significantly reduced total enthalpy rates with reduced cooling requirements, possibly less disassociation, and lower velocities (enhanced mixing and combustion performance, including ignition and flame-holding benefits). However, this concept will suffer from an inevitable reduction in thermal efficiency due to the upstream energy extraction (opposite from a conventional turbojet). The so-called deep-cooled turbojet scheme is a variant of the inverse cycle engine, as noted in Ref. 4.

The MHD bypass engine, the specific engine concept examined in this study, is a type of inverse cycle engine that has been proposed for hypersonic airbreathing propulsion.[7–9] In this engine, axial body forces on fluid elements in the engine flowpath are induced by perpendicular, that is, crossed, electric and magnetic fields within the transverse plane. These body forces can lead to flow deceleration (onboard electrical power generation) or provide flow acceleration (onboard electrical power use). The decelerator and accelerator in the MHD engine are analogous to the (mechanical) turbine and compressor of the conventional turbojet, that is, fundamentally they are work interaction devices and must be treated analytically from that standpoint.

This paper provides a detailed investigation of the performance of the MHD bypass engine. In the next section the absolute and general dependence of the engine specific impulse and specific thrust on total pressure ratio across a general engine flowfield is described. This background is important because the MHD engine, as a type of inverse cycle engine, has an inevitable cycle-related decrease in total pressure across the engine that is completely independent of flowpath irreversibilities. Then a detailed look is provided at this cycle-related loss in total pressure for ideal (no irreversibility) inverse cycle engines and performance losses related to that cycle-related loss. The inevitable MHD-generated irreversibility is then quantified; this irreversibility provides an additional total pressure decrease through the engine in addition to the inverse cycle loss examined in the earlier section. This quantification is done by examining the ideal MHD bypass engine. Here, ideal refers to the fact that only the irreversibility inherent in the MHD work interaction processes is examined. The next three sections use simplifying assumptions regarding constant specific heats and heat release. The subsequent section is a summary of a detailed study of MHD work interaction on the basis of the second law of thermodynamics. This section provides the necessary clarification of the fluid/thermodynamic envelope permitted for the selection of MHD parameters used for high-speed work interaction. Finally, the last section is a summary of a full comparative study of the performance of MHD bypass engines and scramjets at a range of flight Mach numbers. This study is based on engine flowfields that incorporate variable specific heats, inlet shocks, hydrogen–air finite-rate chemistry, friction, wall cooling, etc. In this section, a direct comparison is made between the two engine types for the following quantities: 1) irreversible generation of entropy through the engines in terms of individual component, 2) overall total pressure losses through the engines, 3) engine specific impulses, 4) engine specific thrusts, and 5) overall heat load.

General Engine Performance in Terms of Total Pressure and Heat Input

The following equations detail the specific thrust and the specific impulse of a general (single-stream) engine in terms of the total pressure ratio across the engine (exit to inlet) and the heat input in the engine (assuming engine inflows are known). The equations are not analytical, that is, they are transcendental; however, they are easily solved using a computer. They are provided here to emphasize the influence of total pressure and temperature changes through the flowpath on engine performance.

The general expression for the specific thrust of an airbreathing engine (nondimensionalized by the ambient speed of sound) with or without work interactions, that is, compressors, turbines, deceleration modules, acceleration modules, etc., can be written as follows (where conditions at freestream, 0, are the same as conditions at engine entrance, i):

$$(F/\rho uA)/a_0 = M_0\big[(1+f)(u_e/u_i) - 1 + (1+f)\big(1/\gamma M_e^2\big)(u_e/u_i) - \big(1/\gamma M_0^2\big)(A_e/A_i)\big] \tag{1}$$

where

$$\frac{u_e}{u_i} = \frac{M_e}{M_0}\sqrt{1+\frac{Q}{C_P T_{ti}}}\sqrt{\frac{1+[(\gamma-1)/2]M_0^2}{1+[(\gamma-1)/2]M_e^2}} \tag{2}$$

and M_e is solved for in the following expression:

$$M_e\big\{1+[(\gamma-1)/2]M_e^2\big\}^{-(\gamma+1)/2(\gamma-1)} = M_0(1+f)\big\{1+[(\gamma-1)/2]M_0^2\big\}^{-(\gamma+1)/2(\gamma-1)} \times \sqrt{1+Q/C_P T_{ti}}(A_i/A_e)(P_{ti}/P_{te}) \tag{3}$$

$$\frac{Q}{C_P T_{ti}} = \frac{fh}{C_P T_0\big\{1+[(\gamma-1)/2]M_0^2\big\}} \quad \text{for} \quad f \le f_{\text{stoichimetric}} \tag{4}$$

$$\frac{Q}{C_P T_{ti}} = \frac{f_{\text{stoichimetric}}h}{C_P T_0\big\{1+[(\gamma-1)/2]M_0^2\big\}} \quad \text{for} \quad f > f_{\text{stoichimetric}} \tag{5}$$

The specific impulse I_{sp} is then given as

$$I_{\text{sp}} = [(F/\rho uA)/a_0][a_0/(fg_0)] \tag{6}$$

For H_2 in air, h is approximately 1.2×10^8 J/kg(fuel).

Note that these general relationships imply the direct functional dependence of specific thrust and specific impulse I_{sp} as

$$(F/\rho uA)/a_0 = \text{funct}(M_0, \gamma, f, A_e/A_i, Q/C_P T_{ti}, P_{te}/P_{ti}) \tag{7}$$

$$I_{\text{sp}} = \text{funct}(M_0, \gamma, f, A_e/A_i, Q/C_P T_{ti}, P_{te}/P_{ti}, a_0, g_0) \tag{8}$$

From these fundamental and general relationships, it can be easily shown that total pressure reductions in an engine, regardless of

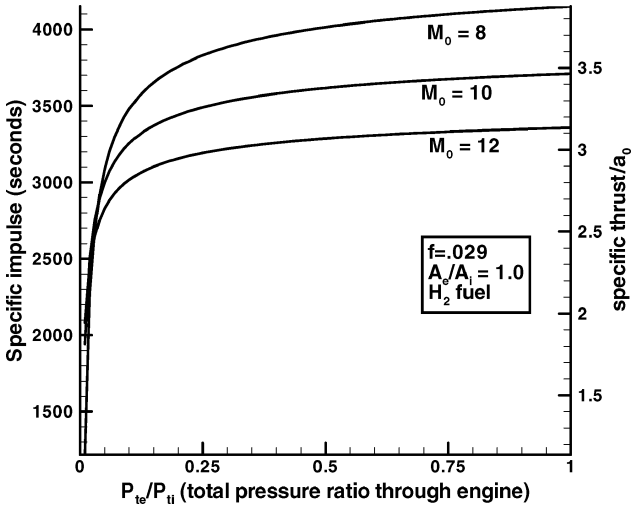

Fig. 1 Specific impulse and specific thrust dependence on total pressure decrease through engine.

source or cause, always negatively impact vehicle thrust and specific impulse. Conversely, total temperature increases always positively impact vehicle performance. Of course, the two parameters (total temperature and pressure) are often related because actual heat release (total temperature increases) occurs with irreversibility (total pressure reduction). Figure 1 shows the general dependence of specific impulse and the nondimensionalized specific thrust for three different flight Mach numbers vs overall total pressure decrease through the engine. Here the fuel–air ratio f is chosen as stoichiometric for H_2–air combustion. (Temperature limits in the engine are not mandated.) A very significant result seen in Fig. 1 is that for large total pressure decreases, that is, very low P_{te}/P_{ti}), the specific impulse decreases exponentially. High-speed airbreathing engines inevitably have very large total pressure decreases due to significant flow losses occurring in the flowpath of the engine. This result will figure prominently as the MHD bypass engine analysis is further developed in subsequent sections of this paper.

Evaluation of the Performance of the Ideal Inverse-Cycle Engine

In this section, the performance of the ideal ram/scramjet and the ideal inverse-cycle engine will be examined. As stated in the Introduction, the MHD bypass engine is a type of inverse-cycle engine: It is, therefore, advantageous to study performance issues for the ideal inverse-cycle engine before further specializing to the MHD bypass engine. It is obvious that the performance obtained using ideal assumptions ignores a large number of critical issues such as total pressure losses associated with flow-path irreversibilities. These effects, of course, largely determine actual engine performance. In this paper, irreversibility losses will be dealt with in subsequent sections. However, it is instructive to first examine the ideal inverse engine and the ideal ram/scramjet. This is done to gain a complete understanding of any inherent total pressure and total temperature drivers within the flowpath for the general engine cycles under consideration. For instance, if an ideal cycle has an inherent total pressure decrease, this is an inevitable performance driver that will occur in the actual nonideal engine. Such a loss should be thoroughly understood and accounted for before additional losses due to irreversibility are studied.

For this section, the term ideal engine refers to an engine in which all components are ideal, that is, inlet, work interaction components, and nozzle are all isentropic. Furthermore, the heat addition process in the combustor is treated as complete and reversible. Such assumptions lead to the permissible upper limits on performance for any given engine type. Further simplifications, standard in any ideal cycle analysis, are made to streamline this particular part of the study: These assumptions include small fuel–air ratios and constant thermodynamic properties. Again, these assumptions will be

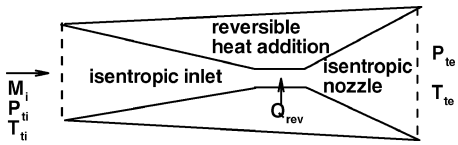

Fig. 2 Ideal ram/scramjet schematic.

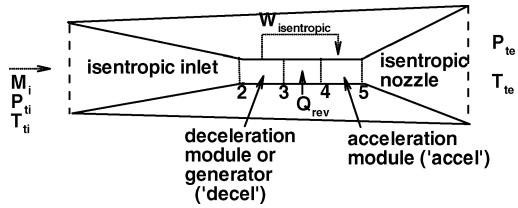

Fig. 3 Ideal inverse cycle schematic.

removed in later sections. Note that the absolute optimal energy addition/extraction corresponds to isentropic work interaction. No energy removal or addition, whether MHD based or not, can outperform an isentropic work interaction.

Consider an ideal ram/scramjet (Fig. 2). Here, the inlet and the nozzle are isentropic (both adiabatic and reversible, implying, among other things, frictionless and shockless). The heat addition process in the combustor is considered reversible from the standpoint of the flowpath. (This implies zero Mach number heat addition where total temperature is equal to the static temperature.)

From the energy equation and second-law considerations,

$$T_{te} = T_{ti} + Q/C_p, \qquad P_{te} = P_{ti} \tag{9}$$

Now, consider an ideal inverse cycle engine (Fig. 3) in which energy is isentropically extracted upstream of the ideal burner and is completely returned to the flow downstream of the burner, again in isentropic work-interaction processes. The inlet and nozzle are assumed to be isentropic. The work interaction is assumed to be complete, that is, no energy losses external to the flowpath between upstream and downstream devices are considered.

From first-law considerations, $T_{te} = T_{ti} + Q/C_p$ because the work interactions in the flowpath are equal and opposite. The total temperature ratio through the engine can then be written as

$$T_{te}/T_{ti} = 1 + Q/C_p T_{ti} \tag{10}$$

To develop an expression for the total pressure ratio through the engine, consider first the work extraction region where W is the work per mass removed from the upstream component. Here, because the flow is isentropic, the total pressure ratio through both the inlet and the upstream work extraction region is given as

$$P_{t3}/P_{ti} = (1 - W/C_p T_{ti})^{\gamma/(\gamma-1)} \tag{11}$$

Furthermore, through the burner,

$$P_{t4}/P_{t3} = 1.0 \tag{12}$$

and through the downstream isentropic work addition device and isentropic nozzle,

$$\frac{P_{te}}{P_{t4}} = \left(\frac{1 + Q/C_p T_{ti}}{1 - W/C_p T_{ti} + Q/C_p T_{ti}}\right)^{\gamma/(\gamma-1)} \tag{13}$$

Now define the energy bypass ratio as follows:

$$\beta = W/C_p T_{ti} \tag{14}$$

This describes the magnitude of energy (work per mass of air) removed from the upstream flow as a fraction of the entering (freestream) total enthalpy per mass of air. The energy bypass ratio must, of course, be less than one.

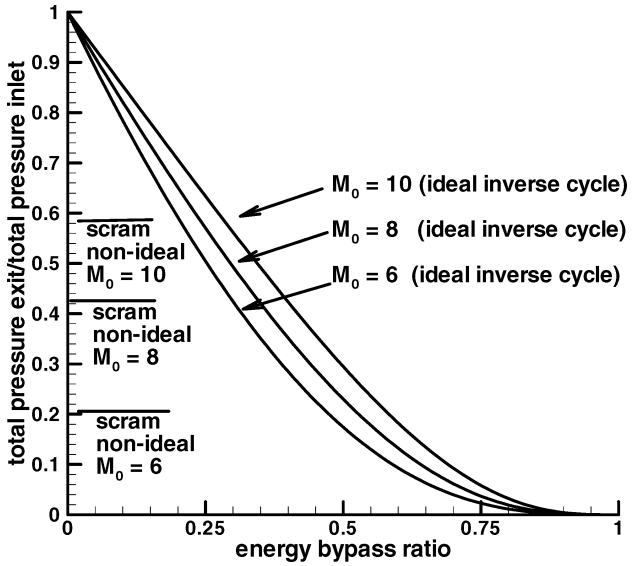

Fig. 4 Total pressure ratio through ideal inverse-cycle engine as a function of energy bypass ratio.

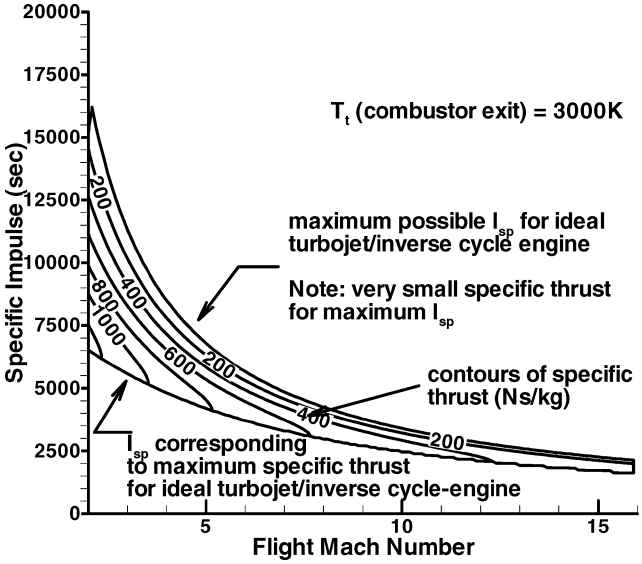

Fig. 5 Specific thrust contours in I_{sp} vs flight Mach number envelope for ideal airbreathing engines.

Next define the overall total pressure ratio through the engine in terms of the bypass ratio:

$$\frac{P_{te}}{P_{ti}} = \left[1 - \frac{(Q \cdot \beta)/C_p T_{ti}}{1 - \beta + Q/C_p T_{ti}}\right]^{\gamma/(\gamma-1)} \tag{15}$$

An examination of this expression demonstrates that the ideal inverse-cycle engine suffers an inevitable total pressure decrease through the engine. This total pressure decrease becomes larger with increasing energy bypass percentage. This is not surprising from the thermal efficiency standpoint because heat is being added at lower temperatures and pressures due to upstream total enthalpy removal. Note that a standard turbojet cycle in which energy is added upstream of the burner and extracted downstream of the burner can also be analyzed using this methodology of analysis and shows an inevitable increase in total pressure through the engine (at least in the ideal case). The total pressure ratios as obtained from the preceding equation for ranges of bypass ratios and engine flight Mach numbers are plotted in Fig. 4 to demonstrate this issue. For Fig. 4, the amount of heat added in the burner was based on stoichimetric hydrogen–air combustion, that is, $f = 0.029$, such that

$$\frac{Q}{C_p T_{ti}} = \frac{fh}{C_p T_0 \left\{1 + [(\gamma-1)/2]M_0^2\right\}} \tag{16}$$

Thus, for instance, for a flight Mach of 10 and an energy bypass ratio of 0.5, the inevitable ideal flow total pressure drop in the inverse-cycle engine corresponds roughly to the total pressure drop experienced through a normal shock at a freestream Mach number of 3.2.

Also shown in Fig. 4 are three vertical lines that correspond to the total pressure drops experienced for nonideal scramjets with heat addition equal to the inverse-cycle engines at the same flight Mach number (as indicated). The single nonideal process allowed in the scramjet cases shown here is supersonic heat addition, (that is, Rayleigh losses, which are defined here as losses associated with heat addition at finite Mach number, are incorporated into the flow. For these cases, the flow was just brought to choking by the given amount of heat addition in each case. As an example, a nonideal scramjet (as defined) at a flight Mach of 8.0 would suffer a drop in total pressure of about 58%. Hence, for the ideal inverse-cycle engine at flight Mach of 8.0, any energy bypass ratio larger than approximately 30% would suffer a proportionally greater total pressure drop than the nonideal scramjet. This is due solely to the inherent performance loss associated with the ideal cycle. Neither inverse-cycle engine nor scramjet have any temperature limits imposed at this point.

Note that such a comparison is unfair to the scramjet flowfield that is developed with the very significant Rayleigh loss (heat addition or combustion at finite Mach number), whereas the inverse cycle results are ideal in every way. Even so, as can be seen from Fig. 4, performance losses for the ideal cycle engine are already significant, and these losses involve the base cycle, not irreversibilities, which are not yet accounted for. Hence, whatever the merits or lack of merits of the inverse-cycle engine (or any of its derivatives such as the MHD engine), one thing is certain: The ideal inverse-cycle engine has a large inherent total pressure drop due to the energy bypass, which is fundamental and is not recoverable. This total pressure drop increases rapidly with increasing bypass ratio. If this total pressure drop combined with the drop due to inevitable irreversibilities in the actual inverse-cycle engine is greater than that experienced by an equivalent scramjet with all of its losses, performance of the inverse-cycle engine in terms of thrust and specific impulse will be less than that of the scramjet.

Because the central idea of the inverse-cycle engine is thermal management, it is instructive to hold the temperature at burner exit at a constant value (chosen here as 3000 K) in Eq. (15) and to vary the bypass ratio and Mach number to calculate resulting specific impulses and specific thrusts for the ideal engine. Figure 5 is the resulting I_{sp} envelope obtained vs flight Mach number. In Fig. 5, the upper (limiting) line defines the maximum possible I_{sp} that is able to be obtained with the ideal inverse cycle. Contours of specific thrust in Ns/kg at various Mach numbers and bypass ratios are plotted below this line. As can be seen, the maximum possible I_{sp} line (upper edge of the envelope) corresponds to zero specific thrust (which is not a desirable situation). The lower (limiting) line, defining the bottom of the displayed I_{sp} envelope, corresponds to maximum specific thrust and is arguably a better estimation of the practical maximum I_{sp} for the ideal inverse cycle. In any event, the actual I_{sp} and specific thrust in a real inverse-cycle engine will always be lower than the values shown for the ideal inverse cycle due to irreversibilities that are not accounted for in this section.

Figure 6 is a companion plot of the same I_{sp} envelope except that the corresponding bypass ratios (rather than specific thrust contours) are shown in the form of contours within the I_{sp} envelope. For instance, for a bypass ratio of zero (corresponding to the ram/scramjet), a maximum possible I_{sp} of about 4000 s occurs at approximately flight Mach of 7. However, at that point, the allowed heat addition in the burner has been reduced to zero due to the imposed temperature limitation of 3000 K in the engine. Therefore, this reduces the specific thrust to zero as indicated on Fig. 5. As flight Mach number is reduced from 7 and holding the bypass ratio at zero, maximum specific thrust is eventually obtained at a flight

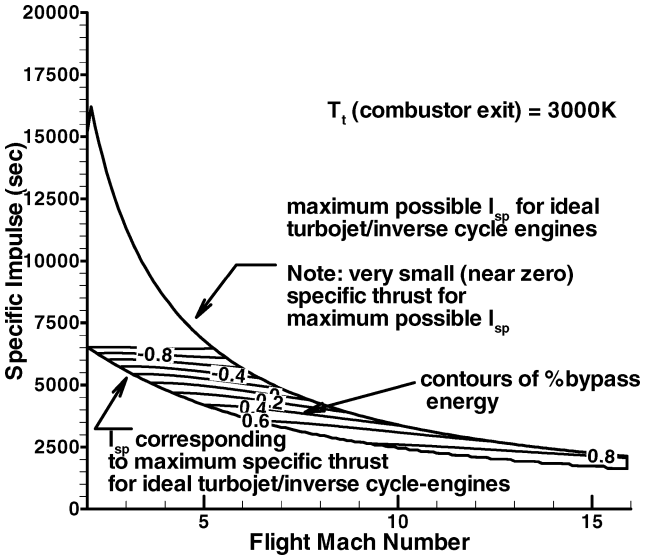

Fig. 6 Bypass ratio contours in Isp vs flight Mach number envelope for ideal air-breathing engines.

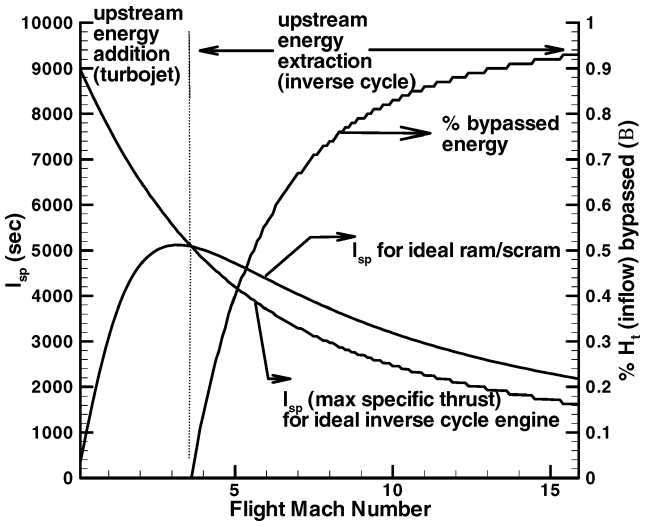

Fig. 7 I_{sp} and bypassed energy vs flight Mach number for maximum thrust for ideal airbreathing engines (also shown is I_{sp} for ideal ram/scram); $T_{t(\text{combustor exit})}$ = 3000 K (variable f).

Mach of around 3.5, where the I_{sp} is about 5000 s. For the inverse-cycle case with bypass ratio of 0.4, maximum I_{sp} (but zero specific thrust) occurs at slightly less than Mach 10. Significantly, even for the ideal engine (as will also be shown later when losses are considered), this indicates that no bypass ratio less than 0.4 will work at flight Mach 10, as long as the temperature limit is held in the burner. Finally, lines of negative bypass ratio in Fig. 6 correspond to the turbojet cycle. This demonstrates the seamless ideal cycle performance from turbojet to ram/scram to inverse-cycle engines. Note that Figs. 5 and 6 are for the ideal inverse-cycle engine. As already mentioned, actual I_{sp} and thrusts will be less (actually considerably less) than these maximum possible theoretical limits.

Figure 7 is an extraction of information from Figs. 5 and 6. In Fig. 7, the lower (limiting) line of the I_{sp} envelope (that corresponding to maximum specific thrust) in Figs. 5 and 6 is separately plotted vs both I_{sp} and the corresponding bypass ratio necessary. The turbojet range (upstream work addition/downstream work extraction) and the inverse-cycle engine range (downstream work addition/upstream work extraction) are clearly shown in Fig. 7. Also shown for reference is the I_{sp} for an ideal ram/scramjet vs flight Mach number with the same heat added in the burner as the inverse-cycle engine at the same flight Mach number. However, for the ideal ram/scramjet, no

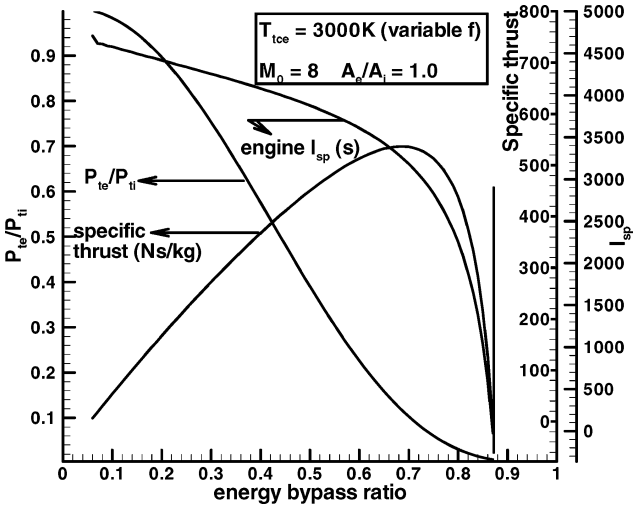

Fig. 8 Inverse cycle engine performance at flight Mach 8, $T_{t(\text{combustor exit})}$ = 3000 K (variable f).

temperature limitation was imposed in the engine. Note that, as expected, the I_{sp} for the ideal ram/scramjet is higher across the Mach number range than the corresponding ideal inverse cycle, due to the earlier discussed inherent total pressure drop associated with the inverse cycle itself.

Figure 8 is energy bypass ratio (at flight Mach of 8 and temperature at end of burner of 3000 K) vs three parameters for the ideal inverse engine: total pressure decrease, specific thrust, and engine I_{sp}. As shown before, the total pressure ratio through the engine decreases rapidly with increasing energy bypass ratio. Note that because the temperature is fixed at burner exit, fuel–air ratios, that is, heat release, are changing with bypass ratio, that is, low bypass ratios mandate low heat release, whereas high bypass ratios allow relatively larger heat release. Figure 8 clearly demonstrates the trade between engine I_{sp} and specific thrust for the inverse engine. At low bypass ratios, I_{sp} is high because total pressure losses are relatively low, but the specific thrusts are very low because very little heat can be added due to the imposed temperature limitation. At higher bypass ratios, specific thrust has a maximum, but I_{sp} is low due to the total pressure decrease associated with the inverse cycle. For larger bypass ratios, the total pressure decrease simply becomes too large, and both impulse and thrust begin to drop exponentially. Again, note that these results are qualitative because only the ideal cycle is being considered: When losses are considered, all performance numbers will go down and actual performance envelopes will be expected to contract dramatically.

If the temperature limitation is eliminated, that is, no temperature limit is imposed throughout the flow-field, the total pressure, specific thrust, and engine specific impulse vs bypass ratio display the characteristics seen in Fig. 9. Here, a fixed heat release, that is, fixed fuel–air ratio, was used across the board. As expected, without a temperature limitation, there is no reduction in specific thrust at lower bypass ratios. Clearly then, for the ideal cycle, relaxing the temperature criteria in the inverse cycle engine simply drives the bypass ratio for optimal performance back to the ideal ram/scramjet (zero bypass ratio) case. However, for reasonable temperature limits in the burner (the central attraction of the inverse engine to begin with), the necessity to achieve reasonable specific thrusts drives the necessary bypass ratio to large values, which in turn are associated with large total pressure decreases and inevitable decreases in engine I_{sp}. The window for the ideal inverse-cycle engine narrows considerably as flight Mach number is increased, as is shown in Fig. 10, in which total pressure, specific thrust, and I_{sp} are plotted vs bypass ratio for fixed combustor exit temperature and flight Mach of 10. Furthermore, it is to be expected that when irreversibilities (losses) associated with large amounts of work interaction between surroundings and flowpath are considered, total pressure losses will increase dramatically. This is because, at the very best, the total

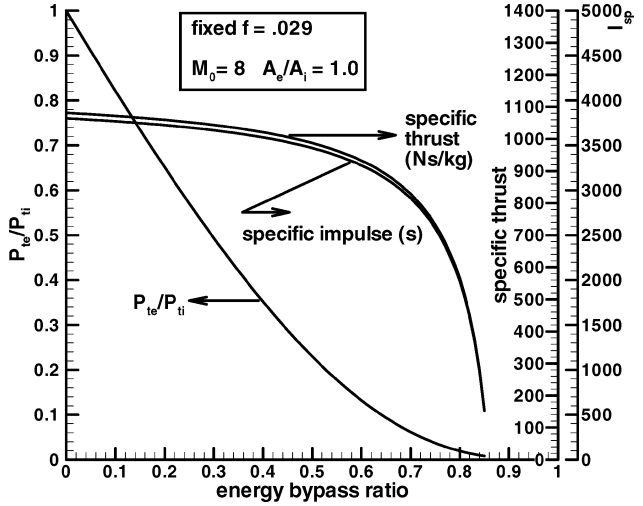

Fig. 9 Ideal inverse cycle engine performance at flight Mach 8; f = 0.029 (no temperature limits).

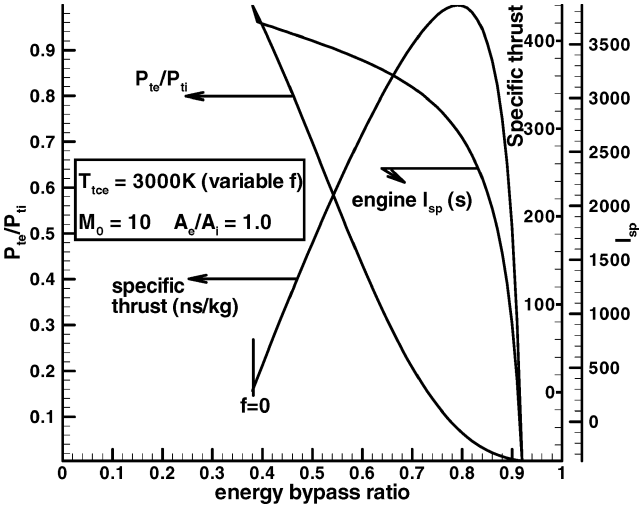

Fig. 10 Ideal inverse cycle engine performance at flight Mach 10; $T_{t(\text{combustor exit})}$ = 3000 K (variable f).

pressure losses associated with irreversible work interaction are expected to scale directly with the amount of energy bypassed. (Bypass ratios of up to 50% and higher have been proposed for the MHD-bypass engine.)

Figure 11 shows a summary of the maximum possible specific impulse that may be achieved by an ideal inverse-cycle engine at three different flight Mach numbers and with a maximum combustor total temperature of 3000 K (variable f). As can be seen, the thermal limit constrains the minimum allowable bypass at high flight Mach numbers to be quite large (40% for Mach 10 and 58% for Mach 12). Bypass ratios below these values could not be achieved while holding the thermal limit at 3000 K.

MHD Engine: Inverse-Cycle Engine with Losses (Irreversibilities)

The MHD engine is a type of inverse engine that specifically utilizes perpendicular, that is, crossed, electric and magnetic fields to 1) decelerate the flow (energy extraction from the flow in the form of generation of electrical power) and 2) accelerate the flow (energy addition to the flow from onboard electrical system). The decelerator (or generator) is upstream of the burner; the accelerator is downstream of the burner.

It was shown in the last section for the ideal inverse cycle in which all work interactions are isentropic that there is an inevitable total pressure decrease across the inverse-cycle engine flowfield

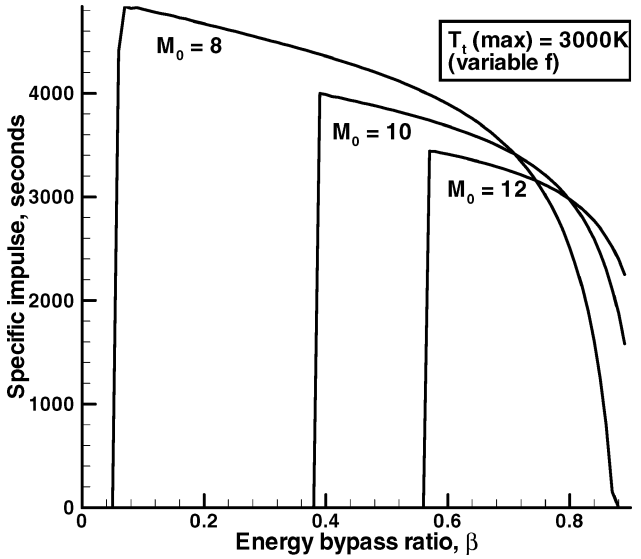

Fig. 11 Ideal inverse-cycle engine performance; specific impulse vs energy bypass ratio β at flight Mach numbers 8, 10, and 12.

that increases rapidly with increased bypassed energy. The question is then posed: For the particular mechanism of MHD, how much more will the total pressure decrease across the engine flowfield be? Additional total pressure decrease will certainly occur due to irreversibilities associated with Joule heating, etc., in the MHD deceleration/acceleration modules. Performance losses from the ideal performance envelopes displayed in the last section will be expected to lower both I_{sp} and thrust levels.

To study this issue in a deliberate manner, let the engine be ideal in every way except that the quasi-one-dimensional version of Maxwell's equations will be incorporated into a quasi-one-dimensional flow solver (see Ref. 10). In other words, the flowfield for the engine will be modeled without friction, without shocks, and with reversible burning. In this way, irreversibilities inherent in the MHD energy interaction process will be isolated and investigated in detail, both in terms of their impact on performance and on their fundamental causes and effects.

The differential equations that describe quasi-one-dimensional flow through the engine or any component (neglecting friction, heat transfer, and Hall currents, all of which would represent additional losses in any event) are as follows:

$$\frac{\mathrm{d}\rho}{\rho} + \frac{\mathrm{d}u}{u} + \frac{\mathrm{d}A}{A} = 0 \tag{17}$$

$$\frac{\mathrm{d}P}{\rho} + u\,\mathrm{d}u = \frac{\sigma_0(E_y - uB)uBA\,\mathrm{d}x}{\rho u A} = \delta w_{\text{eff}} \tag{18}$$

$$C_P\,\mathrm{d}T + u\,\mathrm{d}u = \frac{\sigma_0 E_y(E_y - uB)A\,\mathrm{d}x}{\rho u A} = \delta w_{\text{surr}} \tag{19}$$

$$\frac{\mathrm{d}P}{P} = \frac{\mathrm{d}\rho}{\rho} + \frac{\mathrm{d}T}{T} \tag{20}$$

Note that δw_{surr} is work per mass, which actually crosses boundary (defined as positive to the fluid) and δw_{eff} is work per mass, which is received by the fluid such that

$$T\,\mathrm{d}s_{\text{irr}} = \delta w_{\text{surr}} - \delta w_{\text{eff}} \tag{21}$$

$T\mathrm{d}s_{\text{irr}}$ is, by definition, the differential lost work or internal heat generation in the fluid due to irreversibilities associated with MHD energy interaction. Note, further, that if $E_y = uB$, no energy can be extracted or added to the flow. $E_y < uB$ corresponds to deceleration of the flow (energy extracted from the flow); $E_y > uB$ corresponds to acceleration of the flow (energy added to the flow). A second-law

effectiveness, η, can be readily defined because

$$(uB/E_y)\delta w_{\text{surr}} = \delta w_{\text{eff}} \tag{22}$$

Hence, let

$$\eta = uB/E_y \tag{23}$$

or

$$\eta \cdot \delta w_{\text{surr}} = \delta w_{\text{eff}} \tag{24}$$

Therefore, it is apparent that $\eta < 1$ for acceleration and $\eta > 1$ for deceleration. A more detailed investigation of performance issues arising from the η selection will be discussed in a subsequent section. Simply note here that η of 1.6 for deceleration and η of 0.6 for acceleration provide meaningful second-law performance for the MHD energy interaction. Here η can be described as either the second-law effectiveness or the balancing factor (usually denoted as the load factor in MHD literature) between the imposed electric and magnetic field and the axial fluid velocity. Here it is especially useful to view this parameter from the second-law standpoint.

Analytical Formulation for MHD Engine Performance

The following expression describes the differential total pressure change experienced in a flow in terms of work interaction from or to the surroundings and irreversibility:

$$\frac{\mathrm{d}P_t}{P_t} = \frac{\delta w_{\text{surr}}}{RT_t} - \frac{\mathrm{d}s_{\text{irr}}}{R} \tag{25}$$

and furthermore, by definition, for adiabatic work interaction,

$$C_P\,\mathrm{d}T_t = \delta w_{\text{surr}} \tag{26}$$

When these relationships are used, an expression for the total pressure ratio through the MHD engine can readily be obtained for the ideal MHD engine (where the only loss occurs in work interaction components due solely to MHD work interaction). This expression is as follows:

$$\frac{P_{te}}{P_{ti}} = [1-\beta]^{\gamma x_{\text{decel}}/(\gamma-1)}\left(\frac{1+Q/C_PT_{ti}}{1-\beta+Q/C_PT_{ti}}\right)^{\gamma x_{\text{accel}}/(\gamma-1)} \tag{27}$$

where

$$x = \eta + [(\gamma-1)/2]M_{\text{av}}^2(\eta-1) \tag{28}$$

and M_{av} is the average Mach number in the work interaction process. Note that this represents a mean Mach number for integration purposes to produce Eq. (28).

When this expression for overall total pressure ratio and the earlier expressions for engine specific impulse and specific thrust in terms of total pressure ratio [Eqs. (1–6)] are used, the maximum possible I_{sp} and specific thrust can be plotted for a wide range of conditions for the ideal MHD engine. In particular, it is instructive (as before) to examine the performance for fixed total temperatures at combustor exit, T_{t4}, such that the following relationship between heat, bypass ratio, and maximum temperature is obtained:

$$Q/C_PT_{ti} = T_{t4}\big/T_0\big\{1+[(\gamma-1)/2]M_0^2\big\} + \beta - 1 \tag{29}$$

Figure 12 is energy bypass ratio vs I_{sp} and specific thrust/a_0 for the ideal MHD engine at flight Mach of 8.0 and a total temperature at combustor exit of 3000 K. Average deceleration and acceleration Mach number were held constant at 2.0 in this analysis, and η (the second-law effectiveness) was set at 1.6 for the deceleration region and 0.6 for the accelerator. Note that no solutions (with positive performance) exist for this particular maximum temperature for any bypass ratio for flight Mach numbers of 10.0 or 12.0 due to the total pressure losses incurred in the engine associated with 1) inverse-cycle effects and 2) inherent MHD-generated irreversibilities. At low bypass ratios, little heat can be added due to the imposed thermal limit; the total pressure losses associated with MHD interaction, hence, overwhelm the performance such that the I_{sp} and specific thrust go to zero. At high bypass ratios, total pressure losses are predominant and drive the performance down. Figure 13 is a similar plot for which the total temperature (combustor exit) has been increased to 4000 K. No feasible solution exists for Mach 12. Figure 14 is a similar plot at a temperature of 5000 K and yields positive performance for all Mach numbers for certain bypass ratios. Figures 12–14 show the maximum possible performance of the MHD engine because no friction or irreversibilities other than that associated with MHD itself are considered.

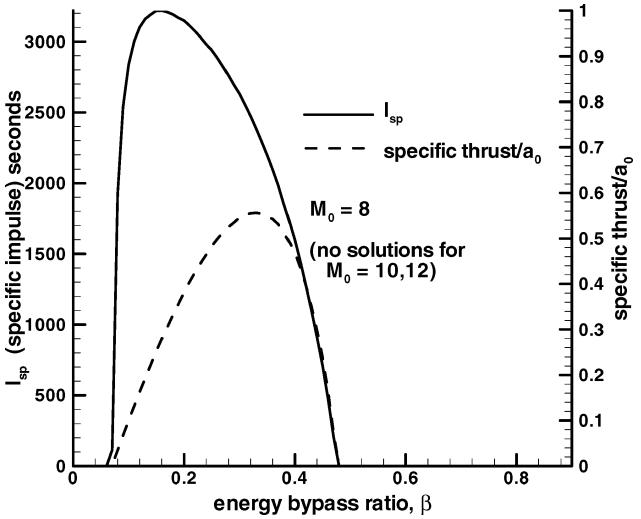

Fig. 12 Engine performance limits for ideal MHD engine; energy bypass ratio β vs I_{sp} and specific thrust, $T_{t(\text{combustor exit})}$ = 3000 K.

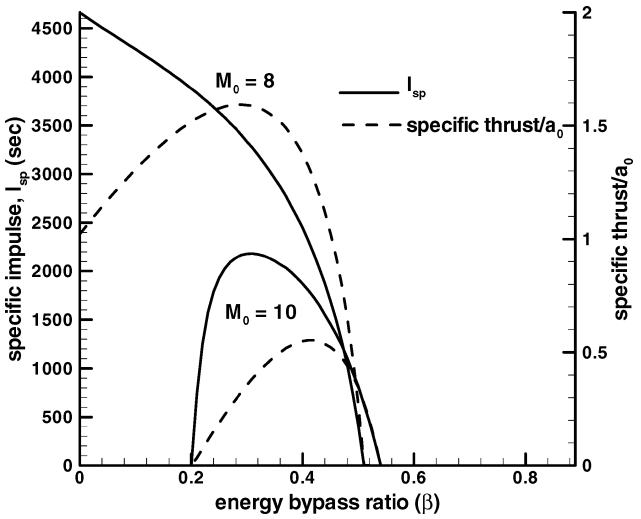

Fig. 13 Engine performance limits for ideal MHD engine; energy bypass ratio β vs I_{sp} and specific thrust, $T_{t(\text{combustor exit})}$ = 4000 K.

Quasi-One-Dimensional Ideal MHD Simulations

Flow Behavior in the Decelerator Module Without Friction

Figure 15 shows the axial distribution of the fluid dynamics in a constant-area frictionless MHD decelerator module with the indicated inputs and inflow. These results are obtained by solving the differential series of Eqs. (17–20) using a suitable numerical marching technique. Note that work extraction in either subsonic or supersonic flow at constant cross-sectional area always drives the Mach number toward 1.0. (Interestingly, this is opposite in trend to energy extraction in terms of heat, that is, cooling the flow drives the Mach away from 1.0 on either side of the sonic locus.) As can be seen

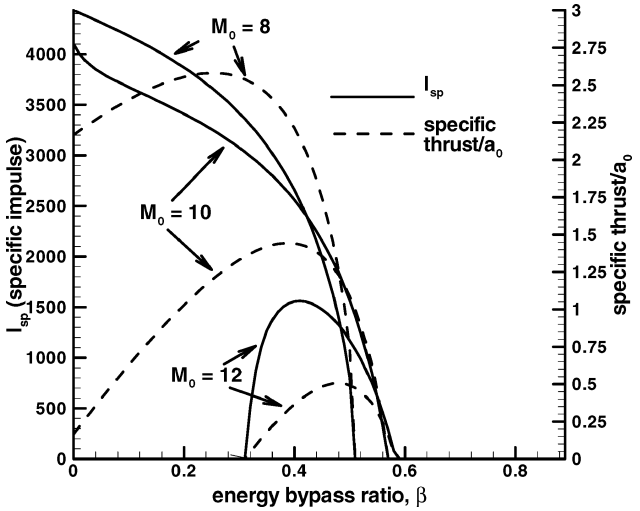

Fig. 14 Engine performance limits for ideal MHD engine; energy bypass ratio β vs I_{sp} and specific thrust, $T_{t(\text{combustor exit})} = 5000$ K.

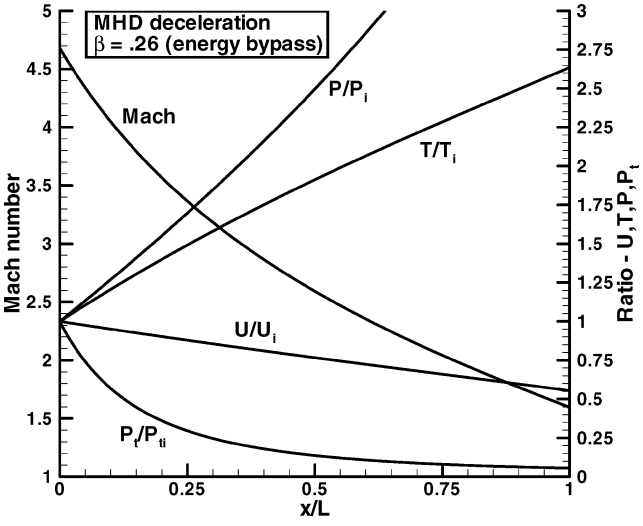

Fig. 15 Example fluid dynamics through MHD decelerator.

by examining Fig. 15, there is a significant entropy increase (due entirely to irreversibility associated entirely with the MHD deceleration) through the decelerator module. This irreversible entropy generation in fact drops the total pressure to 0.05 of its initial value, which is significantly below that of a corresponding isentropic work extraction process (total pressure ratio of 0.35). This loss will figure prominently in reducing engine performance.

Flow Behavior in the Accelerator Module Without Friction

Figure 16 shows the axial distribution of the fluid dynamics in a constant-area frictionless MHD accelerator module with the indicated inputs and inflow. Note that work addition in either subsonic or supersonic flow at constant cross-sectional area always drives the Mach number away from 1.0. There is a significant entropy increase (due entirely to irreversibility associated with the MHD acceleration) through the accelerator module. However, it is somewhat less than the irreversible entropy generation through the decelerator. This is, in fact, true for all cases examined in this investigation. Losses in the decelerator module dominate the overall MHD losses and are often an order of magnitude higher in the decelerator module than in the accelerator module.

MHD Engine Performance Without Friction or Shocks and with Ideal Heat Addition: Quasi-One-Dimensional Results

This section provides three examples of MHD engine (inlet face to engine exit plane) performance using a simple marching code that

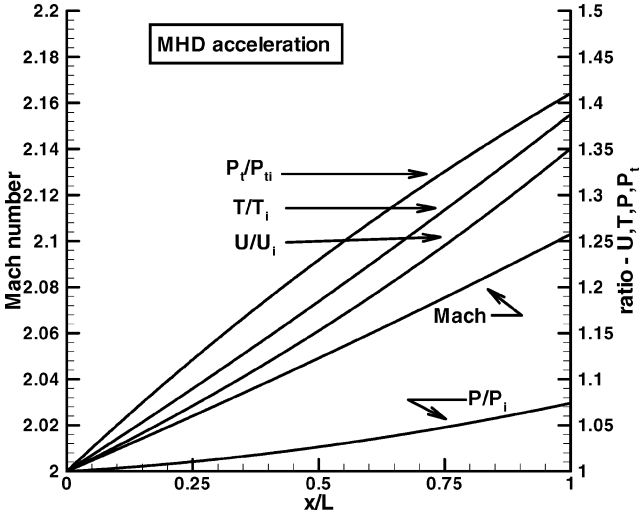

Fig. 16 Example fluid dynamics through MHD accelerator.

solves the differential equations (17–20). These cases provide exact contrasts/comparisons (within the context of numerical solutions) to the analytical results obtained in the preceding section. Recall that the earlier analytical results utilized representative mean Mach numbers in the acceleration module and in the deceleration module. In the cases given later, both decelerator and accelerator have constant cross-sectional area, and varying but reasonable contraction ratios and component lengths are utilized.

Case A

Here $M_0 = 8$, $A_e/A_i = 1.0$, $T_0 = 230$ K, and $f = 0.029$. Electrical conductivity $\sigma_0 = 10$ (both decelerator and accelerator), B (accelerator) $= 2.35$ T and $\eta = 0.473$, and B (decelerator) $= 6.30$ T and $\eta = 1.6$. Energy bypass ratio $\beta = 0.22$, $I_{sp} = 2899$ s, specific thrust $=$ 824 N · s/kg $P_{te}/P_{ti} = 0.0608$ and ΔS_{irr} (decelerator) $=$ 577.5 J/kg · K and ΔS_{irr} (accelerator) $= 76.4$ J/kg · K. Note that this is entirely consistent because, by definition,

$$P_{te(\text{MHD engine})}/P_{te(\text{ideal inverse engine})} = \exp[-\Delta S_{irr}(\text{total})/R] = 0.10245$$

and because

$$P_{te(\text{ideal inverse engine})}/P_{ti} = 0.593$$

(from earlier ideal inverse engine analysis), therefore, $P_{te(\text{MHD engine})}/P_{ti} = 0.0608$, which corresponds with the direct engine result given earlier.

Case B

Here $M_0 = 8$, $A_e/A_i = 1.0$, $T_0 = 230$ K, and $f = 0.029$. Electrical conductivity $\sigma_0 = 20$ (decelerator) and 10 (accelerator), B (accelerator) $= 1.764$ T and $\eta = 0.473$, and B (decelerator) $= 6.30$ T and $\eta = 0.6$. Energy bypass ratio $\beta = 0.32$, $I_{sp} = 2233$ s, specific thrust $= 635$N · s/kg, $P_{te}/P_{ti} = 0.0248$, and ΔS_{irr} (decelerator) $=$ 714.5 J/kg · K and ΔS_{irr} (accelerator) $= 115.0$ J/kg · K.

Case C

Here $M_0 = 10$, $A_e/A_i = 1.0$, $T_0 = 230$ K, and $f = 0.029$. Electrical conductivity $\sigma_0 = 20$ (decelerator) and 10 (accelerator), B (accelerator) $= 2.754$ T and $\eta = 0.473$, and B (decelerator) $= 6.30$ T and $\eta = 1.6$. Energy bypass ratio $\beta = 0.31$, $I_{sp} = 1870$ s, specific thrust $= 531$ N · s/kg, $P_{te}/P_{ti} = 0.01337$, and ΔS_{irr} (decelerator) $= 917$ J/kg · K and ΔS_{irr} (accelerator) $= 140$ J/kg · K.

It is informative to compare these total pressure losses in the ideal MHD engine with the total pressure losses through normal shocks: this is done in Table 1.

From these examples and the previous analysis, it can be seen that the ideal (frictionless, shockless, reversible heat addition) MHD

Table 1 Comparison of ideal MHD engine total pressure decrease with normal shocks

M_0	β	P_{te}/P_{ti}	Normal shock Mach number for equal P_t drop
8.0	.22	.0608	5.0
8.0	.32	.0248	6.3
10.0	.31	.0134	7.2

engine will experience a significant and inevitable total pressure decrease. This decrease is due to the following two phenomena: 1) inverse cycle (ideal) total pressure decrease and 2) irreversibilities associated with ideal MHD interaction, not including friction or any other losses.

Second-Law Issues and Design Issues in MHD Flowfields

It is necessary to examine in greater detail the quasi-one-dimensional equations with the MHD energy interactions [Eqs. (18) and (19)] to understand fully second-law effects associated with MHD energy interactions in isolation of other losses. Equations (18) and (19) are rewritten here as follows:

$$\frac{\mathrm{d}P}{\rho} + u\,\mathrm{d}u = \frac{\sigma_0(E_y - uB)uBA\,\mathrm{d}x}{\rho uA} = \delta w_{\text{eff}} \tag{30}$$

$$C_P\,\mathrm{d}T + u\,\mathrm{d}u = \frac{\sigma_0 E_y(E_y - uB)A\,\mathrm{d}x}{\rho uA} = \delta w_{\text{surr}} \tag{31}$$

Since

$$\eta = uB/E_y, \qquad \eta \cdot \delta w_{\text{surr}} = \delta w_{\text{eff}} \tag{32}$$

the following expressions can be written:

$$\delta w_{\text{surr}} = R(Bu)^2(1/\eta)(1/\eta - 1) \tag{33}$$

$$\delta w_{\text{eff}} = R(Bu)^2(1/\eta - 1) \tag{34}$$

where

$$R = \sigma_0 A\,\mathrm{d}x/\rho uA$$

Figure 17 is $\delta w/R(Bu)^2$ vs η or both δw_{eff} and δw_{surr}. Here η between 0 and 1 corresponds to acceleration (onboard electrical energy used), and η greater than 1 corresponds to deceleration (onboard electrical energy produced). As η approaches 1 from either side, the electromagnetic work interaction go to zero. Figure 17 allows the analysis of the relative amounts of work actually delivered to (or from) the surroundings from (or to) the fluid in terms of the second-law effectiveness term η.

For deceleration ($\eta > 1$), it can be plainly seen that if $\eta > 2$ the work actually transferred from the flow to the surroundings (corresponding to negative work interaction for this paper) decreases; hence, for sensible operation, η should be less than 2. Note that for $\eta > 1$ (deceleration), δw_{eff} is always greater in magnitude than δw_{surr} and in fact increases steadily with η. The difference (delta) between the effective work and the work received by the surroundings for any given η is exactly that portion of the energy transferred in the MHD body–force interaction that is simply returned to the flow as heat, that is, it is the lost work due to irreversibility associated with MHD interaction. In other words, this lost work is equivalent in effect to a frictional loss occurring in the flow.

For acceleration ($0 < \eta < 1$), as η approaches 0, the work required from the surroundings increases exponentially while the actual work received by the flow increases at a lower rate. This results in a rapidly growing lost work term as η is moved toward 0. (Lost work is the energy transferred from the surroundings as work but ending up as a heat interaction to the flow.)

For both deceleration and acceleration cases, the trade is apparent in Fig. 17 between 1) pushing η close to 1.0 to minimize lost work and 2) away from 1.0 (but not greater than 2.0 in the deceleration case) to increase the actual magnitudes of works achieved in the process. Significantly, the addition of friction to the analysis will tend to drive the selection of η farther away from 1.0 for both acceleration and deceleration. To clarify this point, consider the acceleration device. To obtain a relatively large δw_{eff} over a given differential step, a small η close to 0 must be chosen. However, as seen in Fig. 17, there is a large lost work associated with this η, that is, a very large electrical work input from the surroundings would be required. The alternative is to take a small δw_{eff} at a η close to 1.0, where lost work is small. However, the length of the device would then become (by necessity) very large for a meaningful amount of work received by the flow over the overall length. Hence, when friction is considered, η selection is driven away from 1.0 in both acceleration and deceleration devices. For a given skin-friction coefficient C_f, it can be easily shown for the acceleration case that for

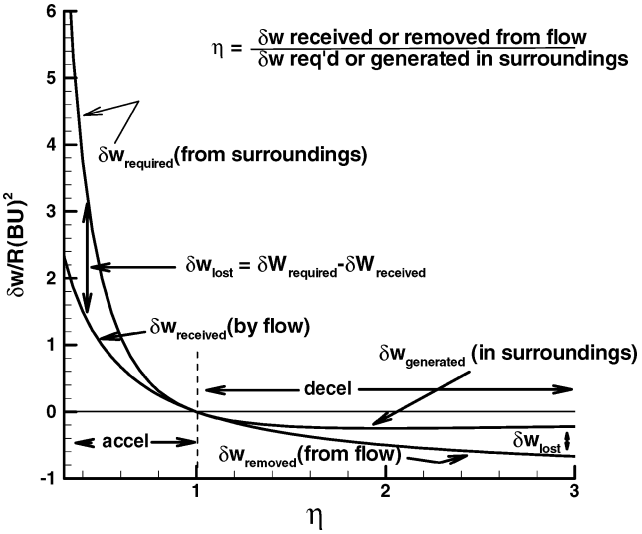

Fig. 17 Second-law characteristics of MHD flow: lost work vs η.

$$\eta > 1\Big/\Big[\big(\rho uAC_f\big/B^2A\sigma_0\big)\sqrt{\pi/A} + 1\Big] \tag{35}$$

more internal work is actually being lost due to friction in the component than is being gained due to positive work interaction received from the surroundings.

It has been found in this study that η of 1.6 for deceleration and η of 0.6 for acceleration yield reasonable results for a range of conditions within the MHD context. Note that η may vary with axial distance along the MHD device but, in this study, is held constant to systemize the analysis.

It can be readily shown that for adiabatic MHD acceleration and deceleration flows, the following expression relates the differential total pressure change across a differential axial step to the differential work interaction, that is, the differential total temperature change:

$$\mathrm{d}P_t/P_t = \gamma/(\gamma - 1)(\mathrm{d}T_t/T_t)(1 - \{1 + [(\gamma - 1)/2]M^2\}(1 - \eta)) \tag{36}$$

It is instructive to examine the impact of the local acceleration or deceleration Mach number on the differential total pressure change for a given differential work interaction by arbitrarily choosing a representative $\mathrm{d}T_t/T_t$ of 0.001 (acceleration) and -0.001 (deceleration) in Eq. (36). This results in Fig. 18, which shows the large decrease in total pressure due to increasing (local) interaction flow Mach number for both acceleration and deceleration cases. Here η are fixed at 1.6 (deceleration) and 0.6 (acceleration). Also shown in Fig. 18 are the isentropic work interaction values for the same $\mathrm{d}T_t/T_t$ In fact, as can be seen from Fig. 18, for the acceleration case, for an interaction Mach of approximately 2.0, total pressure change is zero, whereas for larger Mach numbers it is actually decreasing.

Volumetric Constraints for MHD Deceleration Modules

It can be readily shown that the total volume required for the deceleration module, V_{decel}, is related to the energy bypass ratio β, the second-law effectiveness η, and the average flow Mach number

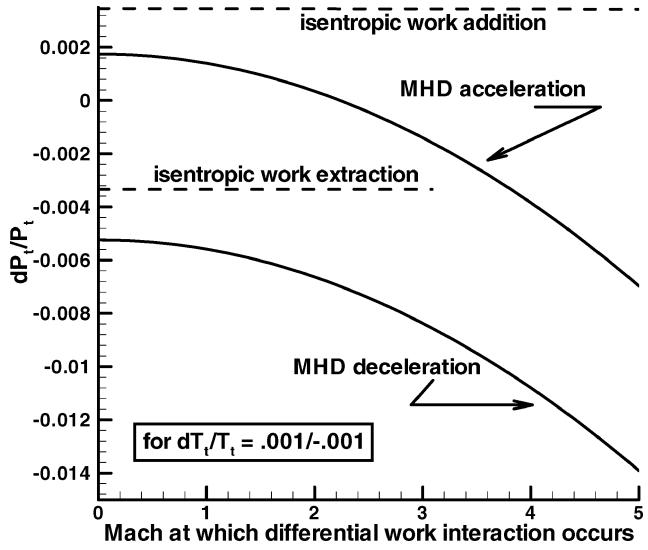

Fig. 18 Example differential total pressure change vs given differential work interaction–flow Mach number dependence.

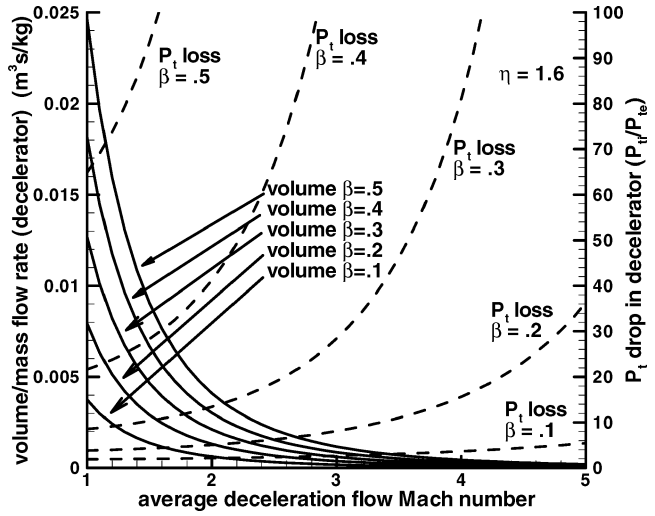

Fig. 19 Decelerator volume and total pressure decrease constraints on MHD deceleration: flow Mach number dependence.

through the decelerator, M, by the following relationship:

$$\ell_n(1-\beta) = V_{\text{decel}}(\gamma-1)\left(\sigma_0 B^2 \Big/ \rho u A\right)(1/\eta)$$

$$\times (1/\eta - 1)M^2\{1 + [(\gamma-1)/2]M^2\} \tag{37}$$

This expression, coupled with the expression for the total pressure ratio through the decelerator,

$$P_{te}/P_{ti} = (1-\beta)^{x\gamma/(\gamma-1)} \tag{38}$$

where

$$x = \eta + [(\gamma-1)/2]M^2(\eta-1) \tag{39}$$

is used to plot (in Fig. 19) both volumetric term V_{decel}/mass flow rate and the total pressure decrease vs the average deceleration Mach number M. Here, $\eta = 1.6$ is used. Results for five bypass ratios ranging from 0.1 to 0.5 are plotted in this figure. There is a disturbingly high degree of constraint on the MHD deceleration process as indicated in Fig. 19. Specifically, for low flow Mach number, very large deceleration volumes are required, that is, decelerator lengths, especially at high bypass ratios. Note that no friction is considered here; however, implicitly, long deceleration lengths (large volume terms) will cause unacceptable frictional and heat transfer losses. Implicit

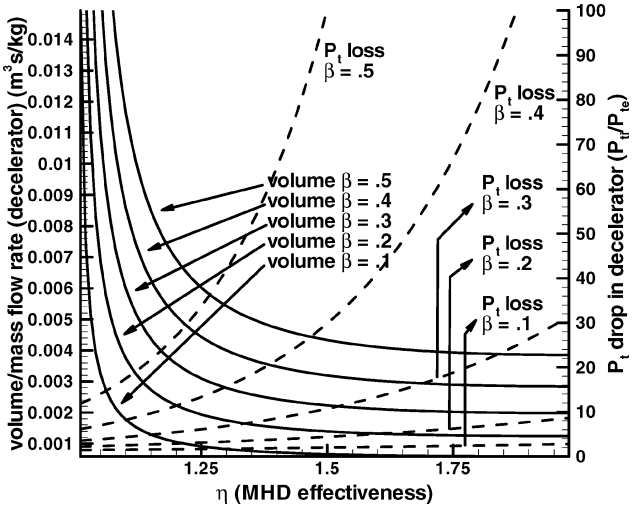

Fig. 20 Decelerator volume and total pressure decrease constraints on MHD deceleration: η dependence.

in the large volumetric term are system weight issues as well. At high flow Mach numbers, the total pressure losses are very large as already discussed, especially for the larger energy bypass ratios. In any event, a flow Mach number of approximately 2 is seen to provide the least undesirable combination of volume/size and fluid total pressure drop for relevant bypass ratios.

Figure 20 shows total pressure decrease and the volumetric term vs η at a fixed deceleration Mach of 2.0. Similar issues to those seen in Fig. 19 and discussed earlier are noted. An η of approximately 1.4 provides the least undesirable combination of volume/size and fluid total pressure drop for relevant bypass ratios. However, actual selection of η will be closer to 1.6 due to frictional effects as already discussed.

Basic Design Issues: MHD Decelerator

It is informative to consider some basic design issues regarding MHD energy interactions. As already noted, Mach number decreases in a constant area deceleration process, that is, both work interaction and friction will drive the Mach toward 1.0. However, considering the downstream requirement of supersonic combustion (which also drives the flow toward Mach 1), it is necessary to maintain reasonable Mach numbers through the MHD deceleration process solely from the existence of the downstream thermal choke constraint in the combustor. This mandates an area increase over the length of the decelerator. The following relationship can be developed, which describes the area ratio (A_e/A_i) necessary in the decelerator to maintain constant Mach number:

$$A_e/A_i = (1-\beta)^{-\gamma x/(\gamma-1)}\sqrt{1-\beta} \tag{40}$$

The required area ratio is in Fig. 21 vs deceleration Mach number and shows the extreme expansions required for even modest energy bypass ratios across the range of Mach number. These ratios are largely unrealistic in an actual vehicle. Even for a bypass ratio of 0.2 and a deceleration Mach number of 2, the area ratio required is about 5. Note that the presence of friction (not considered in this area ratio equation) will further enlarge required area ratios.

It is also possible to find the maximum allowable bypass ratio for a constant area decelerator (the other extreme of this particular design issue) based on choking of the flow at the exit of the decelerator (not considering the downstream combustion, which exacerbates the situation even further). This is plotted in Fig. 22. Again, friction in the decelerator will cause even further reductions in allowable bypass ratio.

Finally, note that the impact of the total pressure loss in the decelerator (due to inverse cycle effects, MHD irreversibility, and frictional and any other losses) on the cross-sectional area required for any downstream thermal throat area is extreme and constrains even

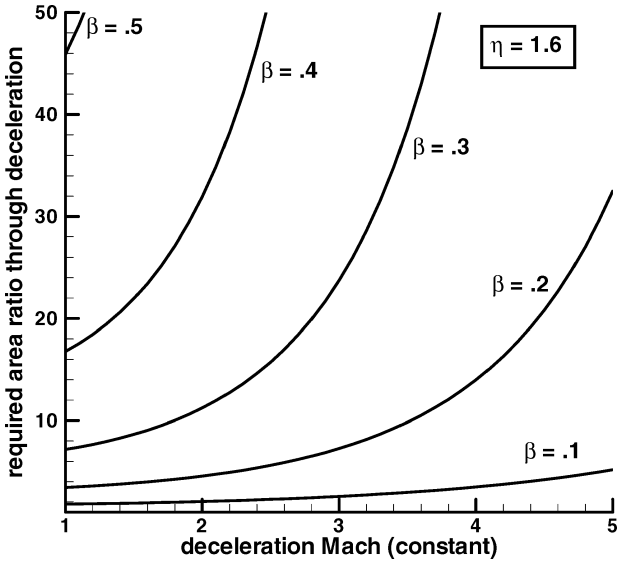

Fig. 21 Required area ratio to hold constant decelerator Mach number.

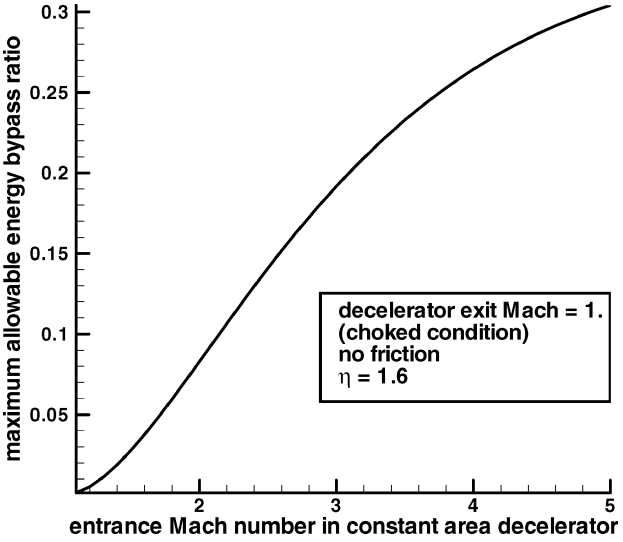

Fig. 22 Maximum allowable energy bypass ratio for constant area decelerator.

further effective use of bypass energy. This is true for either subsonic or supersonic combustion occurring downstream of the decelerator.

Comparative Performance of MHD Bypass Engines and Scramjet Engines: Full Engine Simulations

The preceding analyses for inverse cycle engines and MHD bypass engines are based on constant thermodynamic properties and constant specific heats as well as quasi-one-dimensional fluid dynamics assumed from inlet face to nozzle exit. These earlier sections provide a powerful basis for understanding and diagnosing fundamental losses in MHD flows, as well as the effects of these losses on the expected performance of the MHD bypass engine. This section extends the analysis to incorporate engine flowfields with fluid flow based on variable specific heats, inlet oblique shock systems, fuel system cooling loops (requiring thermally balanced engines), fuel injection effects, skin-friction and wall heat transfer, and finite-rate H_2–O_2 combustor chemistry. Specifically, in this section, the engine flowfield for a vehicle (shown schematically in Fig. 23) is modeled at three different hypersonic Mach numbers for both 1) MHD bypass engine configurations and 2) representative scramjet configurations. The selected Mach numbers for engine evaluation are 8.0, 10.0, and 12.2 at an altitude of 30 km. This is done to compare and clarify performance issues for the two engine types (MHD and scramjet)

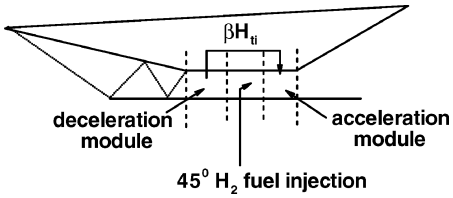

Fig. 23 Schematic of hypersonic engine: MHD and scramjet for flowfield calculations.

in which internal flowpaths are modeled with higher sophistication than in earlier sections. However, all fundamental information already obtained regarding inherent losses in the MHD engine and the permissible second-law operating envelope for the MHD engine has been fully utilized in this section in terms of both constructing the cases examined and explaining the results obtained.

As fully discussed earlier, it is inevitable that the MHD engine will have at least two detrimental performance effects that the scramjet will not experience. These two effects are 1) the total pressure decrease due to the inverse-cycle effect (not related to irreversibility at all) and 2) the total pressure decrease due to irreversibility associated with the MHD acceleration and deceleration (especially the deceleration). In addition, in this particular study, the MHD engine is assumed to be longer (due to the additional modules) and, hence, will have some additional component of skin friction and heat transfer due to these modules. There are also highly restrictive design envelopes involving area ratios and second-law effects on the MHD engine that must be observed in realistic studies.

On the other hand, the scramjet will be expected to have greater combustor irreversibilities due to higher entering total enthalpies, as well as higher heat transfer in the combustor due to relatively higher total enthalpies. Additional mixing enhancement necessary due to higher flow velocities will also increase irreversibilities in the combustor.

This section provides a direct comparison between scramjets and MHD bypass engines at flight Mach between 8 and 12.2 in terms of irreversible entropy generation, overall total pressure decrease, overall heat load, engine specific impulse, and specific thrust.

All cases examined here (both MHD and scramjet) have the following parameters and constraints in common: $T_{\text{wall}} = 1000$ K, $C_{f\,\text{combustor}} = 0.02$, $C_{f\,\text{nozzle}} = 0.005$, inlet shock system with friction, four-shock system with shock cancellation at combustor entrance (two-dimensional inlet), combustor entrance step (entrance area increase), H_2–air mixing, input mixing efficiency distribution, expanding area combustor, quasi-one-dimensional flow in combustor and nozzle, finite-rate H_2–O_2 reaction in combustor (seven species, H_2, O_2, H_20, OH, O, H, and N_2), inlet length = 5 m, combustor length = 0.3 m, nozzle length = 3 m, mach 8 contraction ratio = 10, Mach 10 contraction ratio = 15, Mach 12.2 contraction ratio = 22, Mach 8 fuel equivalence ratio = 0.82, Mach 10 fuel equivalence ratio = 1.1, Mach 12.2 fuel equivalence ratio = 1.34, 45-deg downstream-directed fuel injection at combustor entrance, and thermally balanced engine maintained (fuel used as heat sink).

In addition, for the MHD bypass engine, the following parameters were used: C_f in accelerator/decelerator = 0.005, and length of acceleration/deceleration modules = 0.5 m (constant cross-sectional area). For Mach 8, $\sigma_0 = 10$, B (deceleration) = 8.0, B(acceleration) = 2.45, and β (energy bypass ratio) = 0.202. For Mach 10, $\sigma_0 = 10$, B(deceleration) = 10.8, B(acceleration) = 3.139, and β (energy bypass ratio) = 0.200. For Mach 12.2, $\sigma_0 = 10$, B(deceleration) = 12.0, B(acceleration) = 3.236, and β (energy bypass ratio) = 0.151.

The addition of the MHD modules for the MHD bypass engine increases vehicle length for the MHD cases by a total of 1 m over that of the baseline scramjet. The MHD parameters were selected based on the information described in the preceding sections, that is, $\eta = 1.6$ for the decelerator and $\eta = 0.6$ for the accelerator. There was an inevitable design problem with the MHD engine (discussed in earlier sections) from the standpoint of trying to balance MHD irreversibility losses associated with deceleration at higher Mach

numbers against the tendency of the flow to choke in the accelerator–combustor combination due to the combination of upstream work extraction, frictional effects, and combustion. This design problem was exacerbated by the necessity for reasonably controlling area ratios throughout the engine. In this analysis, constant area MHD devices were mandated, and the supersonic combustor was increased in area to prevent choking. Attempts to slow the flow to subsonic velocities in the MHD combustor resulted in unacceptable area ratios and thermal throat problems. Attempts to increase energy bypass ratios to values significantly greater than those presented here yielded unacceptable irreversibility associated with the deceleration as discussed earlier. Equivalency was maintained (to the degree possible) between MHD bypass engines and scramjets in terms of contraction ratio, fuel equivalence ratio, exit to inlet area ratio, etc.

The inlet simulation is based on first solving the two-dimensional inviscid oblique shock relations with variable specific heats and then including a friction loss estimation based on averaged flow properties in the inlet. Note that the assumptions of the inlet shock system and shock cancellation at the decelerator entrance drives the selection of the contraction ratio of the inlet for all three flight Mach numbers. The simulation technique in the decelerator, combustor, accelerator, and nozzle is based on the marching solution of the following differential equations (modified with the additional MHD terms, as done earlier for constant thermodynamic property studies). This model uses Gordon–McBride curve fits[11] to capture the temperature dependence of the specific heat at constant pressure for multispecies reacting flow. This code also tracks the irreversible generation of entropy due to all mechanisms: friction, heat transfer, mass transfer, finite-rate (nonequilibrium) reaction, and shock waves. Note that for nonadiabatic walls the absolute entropy flux change across a differential step is not equal to the irreversible generation of entropy across that differential step.

Mass:

$$\mathrm{d}(\rho u A) = \mathrm{d}\dot{m}_{\mathrm{fuel}} \tag{41}$$

Momentum:

$$\mathrm{d}(\rho u^2 A + PA) = -\int_{S_w} P\hat{n}_x \,\mathrm{d}S_w - \int_{S_{\mathrm{inj}}} P_{\mathrm{inj}}\hat{n}_x \,\mathrm{d}S_{\mathrm{inj}} - \frac{1}{2}\rho u^2 C_f c \,\mathrm{d}x + u_{\mathrm{inj}}\,\mathrm{d}\dot{m}_{\mathrm{fuel}} + \delta w_{\mathrm{eff}}\rho A \tag{42}$$

Note that $\bar{V}_{\mathrm{fuel}} = u_{\mathrm{inj}}\hat{i} + v_{\mathrm{inj}}\hat{j} + w_{\mathrm{inj}}\hat{k}$.

Energy:

$$\mathrm{d}\left\{\rho u A\left[\sum_{\ell=1}^{\mathrm{NCS}} \alpha_\ell \left(h_{t_{o\ell}} + \int_{T_{\mathrm{ref}}}^{T} C_{p\ell}\,\mathrm{d}T\right) + \frac{u^2}{2}\right]\right\} = \mathrm{d}\dot{m}_{\mathrm{fuel}}\left[h_{t_{o_{\mathrm{fuel}}}} + \int_{T_{\mathrm{ref}}}^{T_{\mathrm{fuel}}} C_{p_{\mathrm{fuel}}}\,\mathrm{d}T + \frac{\bar{V}_{\mathrm{fuel}}\cdot\bar{V}_{\mathrm{fuel}}}{2}\right] + \frac{C_f}{2}\rho u C_{p_{\mathrm{mix}}}(T_w - T_{aw})c\,\mathrm{d}x + \delta w_{\mathrm{surr}}\rho u A \tag{43}$$

where

$$T_{aw} = T + ru^2/2C_{p_{\mathrm{mix}}}$$

and r and NCS are the recovery factor and the number of species present, respectively.

Pressure:

$$P = \rho R T \tag{44}$$

where $R = R_{\mathrm{univ}}/mw_{\mathrm{tot}}$

$$mw_{\mathrm{tot}} = 1\Big/\sum_{\ell=1}^{\mathrm{NCS}} \frac{\alpha_\ell}{mw_\ell}$$

Species:

$$d(\alpha_\ell) = \dot{w}_\ell dx/\rho u \tag{45}$$

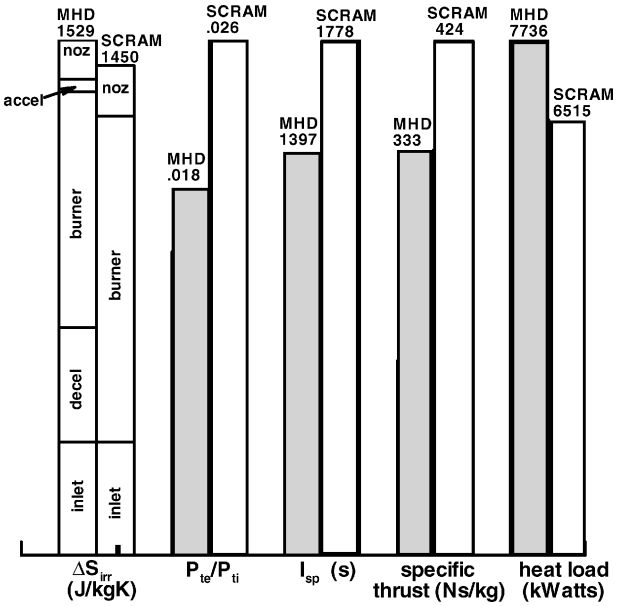

Fig. 24 Comparative summary of engine performance at flight Mach 8.

where $\dot{w}_\ell$ is mass of species ℓ produced per unit time per unit volume (at P, T) due to chemical reactions.

See Eqs. (30) and (31) for the modeled one-dimensional MHD representations for δw_{eff} and δw_{surr} that appear in Eqs. (42) and (43).

Figure 24 is a comparative bar chart of the irreversible generation of entropy, total pressure recovery, overall heat load, specific impulse, and specific thrust for both MHD bypass and scramjet engines at a flight Mach number of 8. The bypass ratio for the MHD engine for this case is 20.2%. The inlet entropy generation is equal between the two engine types. (The same inlet configuration is utilized.) The MHD deceleration has a large entropy increase as shown (26% of the overall irreversibility through the engine); there is no corresponding increment in the scramjet. As expected, the combustor irreversibility for the scramjet is significantly higher than that of the MHD bypass engine (approximately 50% greater). The MHD acceleration has an irreversible entropy generation equal to 4% of the overall engine irreversibility; there is no corresponding increment for the scramjet. The MHD nozzle and scramjet nozzle are roughly the same in terms of irreversibility. The net effect of the irreversible generation of entropy in the two engines results in slightly higher losses for the MHD engine at this Mach number. Note, however, that the MHD engine also experiences an additional total pressure drop due to the energy bypass (inverse cycle effect), unrelated to irreversibility.

The combination of these two effects (slightly greater irreversibility and the inverse cycle effect for the MHD engine) results in the significantly greater total pressure loss shown for the MHD engine in Fig. 24. The effect on engine I_{sp} and specific thrust are also seen in Fig. 24: Note that engine performance is dramatically affected by total pressure differences at low total pressure recovery. (See the exponential drop-off in I_{sp} and thrust at low engine pressure recoveries in Fig. 1.) As can be seen, the I_{sp} for the MHD bypass engine is 1397 s; the I_{sp} for the scramjet engine is 1778 s. The specific thrusts for the two engines are proportional to I_{sp}.

Also shown in Fig. 24 is the overall heat load (heat transferred from flow to fuel to maintain constant wall temperatures). It is seen that the MHD engine has approximately 19% greater overall heat load requirement. This is despite the fact that the MHD engine has a cooler core (total temperature at combustor exit of 3300 K in comparison to the scramjet total temperature of 3631 K). The reason for this is entirely driven by the additional cooling requirements in the decelerator and accelerator modules.

Figure 25 is a similar comparative bar chart for a flight Mach number of 10 with a MHD engine bypass ratio of 20%. Very similar

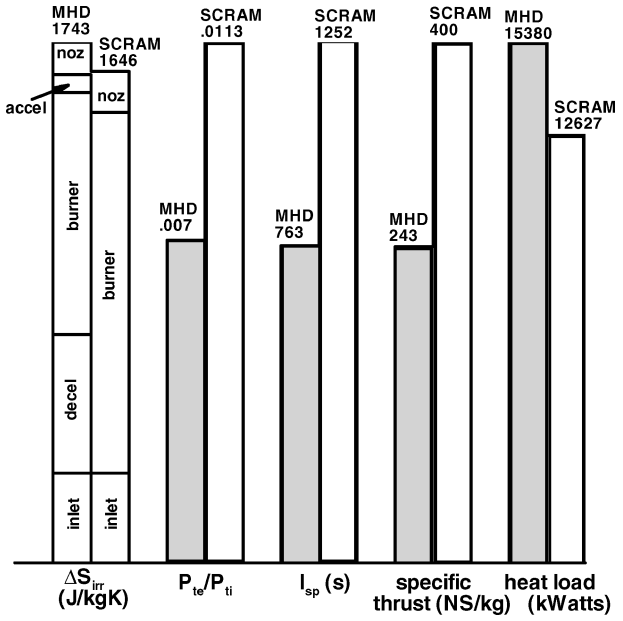

Fig. 25 Comparative summary of engine performance at flight Mach 10.

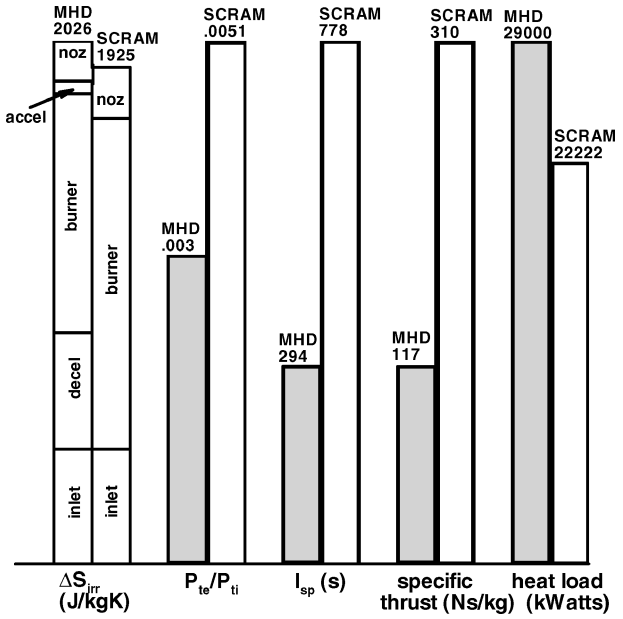

Fig. 26 Comparative summary of engine performance at flight Mach 12.2.

results are seen on this chart: There are more losses. (Note the entropy increments in Fig. 25 are per unit mass and mass flow rate through the engine is substantially greater for higher Mach number flight.) The deceleration module for the MHD engine is responsible for approximately 27% of the overall loss in the engine. MHD engine I_{sp} is 763 s; scramjet I_{sp} is 1252 s. Again, the overall heat load for the MHD engine is about 20% higher due to cooling requirements for the MHD decelerator and accelerator modules. Again, this is despite the cooler combustor realized in the MHD engine.

Figure 26 presents results for a flight Mach number of 12. Here the bypass ratio for the MHD engine was 15%; higher bypass ratios are possible but begin to take an increasing toll in terms of decelerator losses, inverse cycle performance losses, and design constraints. For this case, the total pressure decrease through the MHD engine is very large such that the I_{sp} and thrust are very small. Similar results are obtained as for lower flight Mach numbers: 30% greater overall heat load in the MHD engine, I_{sp} of 294 s for the MHD engine, and I_{sp} of 778 s for the scramjet.

Summary

A detailed analysis of the MHD energy bypass engine that has been proposed for hypersonic airbreathing flight is provided. The central feature of the MHD engine is the extraction of energy from the flowfield within the upstream diffusion process and the return of that energy to the flowfield downstream of the combustor. These energy interactions utilize perpendicular, that is, crossed, electric and magnetic fields in the transverse plane of the flow, which induce body forces such that onboard electrical energy is generated in the upstream decelerator and onboard electrical energy is used in the downstream accelerator. The main purpose of the MHD bypass engine is to allow a cooler and lower Mach number engine core flow, that is, in the combustor, than experienced in a conventional scramjet with attendant benefits in terms of losses and operability. It is seen here that the MHD bypass engine is a specific type of the inverse-cycle engine.

The first section of this paper describes and illustrates the general relationship between engine specific impulse and overall total pressure ratio. It is clearly shown that engines that suffer from very large total pressure decreases, regardless of cause or source, exist in a region of very rapidly decreasing engine specific impulse and specific thrust. The relationship between total pressure and engine performance is important because subsequent analysis of the ideal inverse-cycle engine demonstrates a significant total pressure decrease mandated solely by the inverse cycle itself. This fundamental decrease in total pressure is independent of any irreversibilities that may occur in the flowpath. Furthermore, the total pressure through the engine is shown to decrease exponentially with energy bypassed in the cycle with significant negative consequences on engine performance. The fundamental limits on achievable engine specific impulse and specific thrust using the ideal inverse cycle scheme were also described and illustrated.

A large total pressure decrease through the MHD engine (in addition to that associated with the ideal inverse cycle itself) also occurs due to irreversibility associated solely with the MHD work interactions. This MHD-mandated flow loss is described in terms of effects on engine performance. This is done in the absence of all other irreversibilities to isolate the work interaction losses due to MHD bypass. It is seen that considerable reductions in the performance envelope of the MHD engine occur due to this additional loss. It is also noted that the deceleration (work extraction) region has significantly higher irreversibility than the accelerator.

The thermo-fluid-dynamic characteristics of the MHD work interaction process is analyzed in detail to provide understanding and clarification of issues pertaining to acceleration, deceleration, electric and magnetic field strengths, lost work, and irreversibility. The correct selection of specific parameters for the MHD cases examined in both earlier and later sections is enabled. In particular, the selection of the second-law effectiveness (designated η) drives the acceleration or deceleration of the flow and describes the balance between the field magnitudes (electric and magnetic) and the flow velocity. In addition, this parameter defines the amount of lost work occurring in the MHD work interaction processes, that is, it defines the irreversibility associated with the interaction. It is seen that the total pressure decrease (or entropy rise or increasing lost work) occurring in the decelerator becomes extreme for local flow Mach numbers much above 2.0 and bypass ratios greater than 20%. In addition, the volume (or, equivalently, length) of the accelerator is seen to become excessive for Mach numbers less than 2.0 and any higher bypass ratios. Also shown and discussed are design problems inherent in the MHD engine. These issues include the fact that work extraction at supersonic Mach numbers drives a flow toward choking. This fact, when coupled with thermal choking in the combustor, requires either unacceptably large cross-sectional area variations in the decelerator or severely limits the allowable bypass ratio itself.

A comparison is provided of the MHD bypass engine and the conventional scramjet at three flight Mach numbers ranging from 8 to 12.2. The modeling is based on variable specific heat differential

analysis, oblique shock inlet systems, hydrogen–air finite-rate combustion, fuel injection and mixing, wall cooling with injected fuel used as the heat sink, etc. The analysis demonstrates that irreversibilities associated with the MHD components coupled with the total pressure decrease inherent in the inverse cycle result in lower specific impulses and performance across the Mach number range for the MHD bypass engine in comparison to the conventional scramjet. In addition, because of increased cooling requirements within the accelerator and decelerator modules, the overall heat load of the MHD engine is actually greater across the flight Mach number range than the conventional scramjet. This is true despite the fact that the MHD engine operates at a lower total temperature and velocity in the combustor core due to the upstream energy extraction.

This study is based entirely on flowpath performance and does not include any system or weight penalties associated with either the MHD engine or the scramjet. Although this study indicates that the MHD bypass engine is not attractive in comparison to the conventional scramjet from the standpoint of general engine performance, the generation of some onboard electrical power may in fact be very advantageous even with the large performance penalty described in this investigation. This is because on-board drag reduction systems and flowfield modification systems that require substantial amounts of beamed energy can possibly result in very large reductions in external drag or even increased mass capture for the engine itself. From this standpoint, utilization of MHD deceleration for onboard power generation may yet prove to be an attractive concept.

Acknowledgments

This work was performed in conjunction with NASA Grant NAG1-01122. In particular, gratitude is extended to Charles McClinton of NASA Langley Research Center for his continual encouragement and support and for many fruitful discussions in past years regarding flow losses and scramjet engine performance. Also L. Hunt and D. Petley of NASA Langley Research Center are thanked for their support, patience, and encouragement regarding this study.

References

[1]Riggins, D. W., McClinton, C. R., and Vitt, P. H., "Thrust Losses in Hypersonic Engines," *Journal of Propulsion and Power*, Vol. 13, No. 2, 1997, pp. 281–287.

[2]Riggins, D. W., "Effects of Combustion and Irreversibilities on the Performance of High-Speed Engines," Final Report, NASA Grant NAG1-1189, Aug. 1998.

[3]Riggins, D. W., "The Thermodynamic Continuum of Jet Engine Performance: The Principle of Lost Work due to Irreversibility in Aerospace Systems," *International Journal of Thermodynamics*, Vol. 6, No. 3, 2003, pp. 107–120.

[4]Curran, E. T., "High-Speed Flight Propulsion Systems," edited by S. N. B Murthy and E. T. Curran, Progress in Astronautics and Aeronautics, Vol. 137, AIAA, Washington, DC, 1991, pp. 8–11.

[5]Mordell, D. L., Eyre, F. W., and Sreenath, A. V., "The Inverted Turbojet," *Proceedings of the Eighth Anglo-American Aeronautical Conference*, Royal Aeronautical Society, London, Sept. 1961, pp. 159–180.

[6]Ribaud, Y., "Inverse Cycle Engine for Hypersonic Air-Breathing Propulsion," *Proceedings of the Ninth International Symposium on Air-Breathing Engines*, Vol. 2, AIAA, Washington, DC, 1989, pp. 1044–1050.

[7]Litchford, R. J., Cole, J. W., and Bityurin, V. A., "Thermodynamic Cycle Analysis of Magnetohydrodynamic-Bypass Hypersonic Airbreathing Engines," *Journal of Propulsion and Power*, Vol. 17, No. 2, 2001, pp. 477–480.

[8]Park, C., Bogdanoff, D., and Mehta, U. B., "Theoretical Performance of Frictionless Magnetohydrodynamic-Bypass Scramjets," *Journal of Propulsion and Power*, Vol. 17, No. 3, 2001, pp. 591–598.

[9]Bruno, C., and Czysz, P. A., "An Electro-Magnetic-Chemical Hypersonic Propulsion System," AIAA Paper 98-1582, April 1998.

[10]Hill, P. G., and Peterson, C. R., "Mechanics and Thermodynamics of Propulsion," 1st ed., Addison–Wesley, Reading, MA, 1965, pp. 123–132.

[11]McBride, B. J., Gordon, S., and Reno, M. A., "Coefficients for Calculating Thermodynamic and Transport Properties of Individual Species," NASA Rept. TM-4513, Oct. 1993.